

Symmetry disquisition on the TiOX phase diagram

Daniele Fausti,* Tom T. A. Lummen, Cosmina Angelescu, Roberto Macovez,
Javier Luzon, Ria Broer, Petra Rudolf, and Paul H.M. van Loosdrecht†

*Zernike Institute for Advanced Materials,
University of Groningen, 9747 AG Groningen, The Netherlands.*

Natalia Tristan and Bernd Büchner

IFW Dresden, D-01171 Dresden, Germany

Sander van Smaalen

Laboratory of Crystallography, University of Bayreuth, 95440 Bayreuth, Germany

Angela Möller, Gerd Meyer, and Timo Taetz

Institut für Anorganische Chemie, Universität zu Köln, 50937 Köln, Germany

(Dated: February 8, 2022)

Abstract

The sequence of phase transitions and the symmetry of in particular the low temperature incommensurate and spin-Peierls phases of the quasi one-dimensional inorganic spin-Peierls system TiOX (TiOBr and TiOCl) have been studied using inelastic light scattering experiments. The anomalous first-order character of the transition to the spin-Peierls phase is found to be a consequence of the different symmetries of the incommensurate and spin-Peierls ($P2_1/m$) phases.

The pressure dependence of the lowest transition temperature strongly suggests that magnetic interchain interactions play an important role in the formation of the spin-Peierls and the incommensurate phases. Finally, a comparison of Raman data on VOCl to the TiOX spectra shows that the high energy scattering observed previously has a phononic origin.

PACS numbers: 68.18.Jk Phase transitions

63.20.-e Phonons in crystal lattices

75.30.Et Exchange and superexchange interactions

75.30.Kz Magnetic phase boundaries (including magnetic transitions, metamagnetism, etc.)

78.30.-j Infrared and Raman spectra

I. INTRODUCTION

The properties of low-dimensional spin systems are one of the key topics of contemporary condensed matter physics. Above all, the transition metal oxides with highly anisotropic interactions and low-dimensional structural elements provide a fascinating playground to study novel phenomena, arising from their low-dimensional nature and from the interplay between lattice, orbital, spin and charge degrees of freedom. In particular, low-dimensional quantum spin ($S=1/2$) systems have been widely discussed in recent years. Among them, layered systems based on a $3d^9$ electronic configuration were extensively studied in view of the possible relevance of quantum magnetism to high temperature superconductivity^{1,2}. Though they received less attention, also spin= $1/2$ systems based on early transition metal oxides with electronic configuration $3d^1$, such as titanium oxyhalides (TiOX, with X=Br or Cl), exhibit a variety of interesting properties^{3,4}. The attention originally devoted to the layered quasi two-dimensional $3d^1$ antiferromagnets arose from considering them as the electron analog to the high- T_c cuprates⁵. Only recently TiOX emerged in a totally new light, namely as a one-dimensional antiferromagnet and as the second example of an inorganic spin-Peierls compound (the first being CuGeO_3)^{6,7}.

The TiO bilayers constituting the TiOX lattice are candidates for various exotic electronic configurations, such as orbital ordered³, spin-Peierls⁶ and resonating-valence-bond states⁸. In the case of the TiOX family the degeneracy of the d orbitals is completely removed by the crystal field splitting, so that the only d -electron present, mainly localized on the Ti site, occupies a nondegenerate energy orbital³. As a consequence of the shape of the occupied orbital (which has lobes oriented in the b - and c -directions, where c is perpendicular to the layers), the exchange interaction between the spins on different Ti ions arises mainly from direct exchange within the TiO bilayers, along the b crystallographic direction³. This, in spite of the two-dimensional structural character, gives the magnetic system of the TiOX family its peculiar quasi one-dimensional properties⁶. Magnetic susceptibility⁶ and ESR³ measurements at high temperature are in reasonably good agreement with an antiferromagnetic, one-dimensional spin-1/2 Heisenberg chain model. At low temperature (T_{c1}) TiOX shows a first-order phase transition to a dimerised nonmagnetic state, discussed in terms of a spin Peierls state^{6,9,10}. Between this low temperature spin Peierls phase (SP) and the one-dimensional antiferromagnet in the high temperature phase (HT), various experimental evidence^{4,11,12,13} showed the existence of an intermediate phase, whose nature and origin is still debated. The temperature region of the intermediate phase is different for the two compounds considered in this work, for TiOBr $T_{c1} = 28$ K and $T_{c2} = 48$ K while for TiOCl $T_{c1} = 67$ K and $T_{c2} = 91$ K. To summarize the properties so far reported, the intermediate phase ($T_{c1} < T_{c2}$) exhibits a gapped magnetic excitation spectrum⁴, anomalous broadening of the phonon modes in Raman and IR spectra^{9,13}, and features of a periodicity incommensurate with the lattice^{14,15,16,17}. Moreover, the presence of a pressure induced metal to insulator transition has been recently suggested for TiOCl¹⁸. Due to this complex phase behavior, both TiOCl and TiOBr have been extensively discussed in recent literature, and various questions still remain open: there is no agreement on the crystal symmetry of the spin Peierls phase, the nature and symmetry of the incommensurate phase is not clear and the anomalous first-order character of the transition to the spin Peierls state is not explained.

Optical methods like Raman spectroscopy are powerful experimental tools for revealing the characteristic energy scales associated with the development of broken symmetry ground states, driven by magnetic and structural phase transitions. Indeed, information on the

nature of the magnetic ground state, lattice distortion, and interplay of magnetic and lattice degrees of freedom can be obtained by studying in detail the magnetic excitations and the phonon spectrum as a function of temperature. The present paper reports on a vibrational Raman study of TiOCl and TiOBr, a study of the symmetry properties of the three phases and gives coherent view of the anomalous first order character of the transition to the spin Peierls phase. Through pressure-dependence measurements of the magnetic susceptibility, the role of magnon-phonon coupling in determining the complex phase diagram of TiOX is discussed. Finally, via a comparison with the isostructural compound VOCl, the previously reported^{13,19} high energy scattering is revisited, ruling out a possible interpretation in terms of magnon excitations.

II. EXPERIMENT

Single crystals of TiOCl, TiOBr, and VOCl have been grown by a chemical vapor transport technique. The crystallinity was checked by X-ray diffraction¹². Typical crystal dimensions are a few mm² in the *ab*-plane and 10-100 μm along the *c*-axis, the stacking direction¹⁵. The sample was mounted in an optical flow cryostat, with a temperature stabilization better than 0.1 K in the range from 2.6 K to 300 K. The Raman measurements were performed using a triple grating micro-Raman spectrometer (Jobin Yvon, T64000), equipped with a liquid nitrogen cooled CCD detector (resolution 2 cm⁻¹ for the considered frequency interval). The experiments were performed with a 532 nm Nd:YVO₄ laser. The power density on the sample was kept below 500 W/cm² to avoid sample degradation and to minimize heating effects.

The polarization was controlled on both the incoming and outgoing beam, giving access to all the polarizations schemes allowed by the back-scattering configuration. Due to the macroscopic morphology of the samples (thin sheets with natural surfaces parallel to the *ab*-planes) the polarization analysis was performed mainly with the incoming beam parallel to the *c*-axis (*c*(aa) \bar{c} , *c*(ab) \bar{c} and *c*(bb) \bar{c} , in Porto notation). Some measurements were performed with the incoming light polarized along the *c*-axis, where the *k*-vector of the light was parallel to the *ab*-plane and the polarization of the outgoing light was not controlled. These measurements will be labeled as *x*(*c*★) \bar{x} .

The magnetization measurements were performed in a Quantum Design Magnetic Property Measurement System. The pressure cell used is specifically designed for measurement of the DC-magnetization in order to minimize the cell's magnetic response. The cell was calibrated using the lead superconducting transition as a reference, and the cell's signal (measured at atmospheric pressure) was subtracted from the data.

III. RESULTS AND DISCUSSION

The discussion will start with a comparison of Raman experiments on TiOCl and TiOBr in the high temperature phase, showing the consistency with the reported structure. Afterwards, through the analysis of Raman spectra the crystal symmetry in the low temperature phases will be discussed, and in the final part a comparison with the isostructural VOCl will be helpful to shed some light on the origin of the anomalous high energy scattering reported for TiOCl and TiOBr^{13,19}.

A. High Temperature Phase

The crystal structure of TiOX in the high temperature (HT) phase consists of buckled Ti-O bilayers separated by layers of X ions. The HT structure is orthorhombic with space group $Pm\bar{m}n$. The full representation²⁰ of the vibrational modes in this space group is:

$$\Gamma_{tot} = 3A_g + 2B_{1u} + 3B_{2g} + 2B_{2u} + 3B_{3g} + 2B_{3u}. \quad (1)$$

Among these, the modes with symmetry B_{1u} , B_{2u} , and B_{3u} are infrared active in the polarizations along the c , b , and a crystallographic axes⁹, respectively. The modes with symmetry A_g , B_{2g} , and B_{3g} are expected to be Raman active: The A_g modes in the polarization (aa) , (bb) , and (cc) ; the B_{2g} modes in (ac) and the B_{3g} ones in (bc) . Fig.1 shows the room tem-

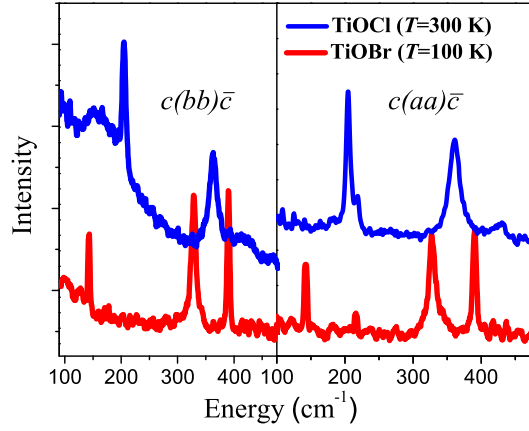


FIG. 1: (Color online) Polarized Raman spectra (A_g) of TiOCl and TiOBr in the high temperature phase, showing the three A_g modes. Left panel: (bb) polarization; right panel: (aa) polarization.

perature Raman measurements in different polarizations for TiOCl and TiOBr, and Fig.2 displays the characteristic Raman spectra for the three different phases of TiOBr, the spectra are taken at 100 (a), 30 (b) and 3K (c). At room temperature three Raman active modes are clearly observed in both compounds for the $c(aa)\bar{c}$ and $c(bb)\bar{c}$ polarizations (Fig.1), while none are observed in the $c(ab)\bar{c}$ polarization. These results are in good agreement with the group theoretical analysis. The additional weakly active modes observed at 219 cm^{-1} for TiOCl and at 217 cm^{-1} for TiOBr are ascribed to a leak from a different polarization. This is confirmed by the measurements with the optical axis parallel to the ab -planes ($x(c\star)\bar{x}$) on TiOBr, where an intense mode is observed at the same frequency (as shown in the inset of Fig.2(a)). In addition to these expected modes, TiOCl displays a broad peak in the $c(bb)\bar{c}$ polarization, centered at around 160 cm^{-1} at 300K; a similar feature is observed in TiOBr as a broad background in the low frequency region at 100K. As discussed for TiOCl¹³, these modes are thought to be due to pre-transitional fluctuations. Upon decreasing the temperature, this "peaked" background first softens, resulting in a broad mode at T_{c2} (see Fig.2(b)), and then locks at T_{c1} into an intense sharp mode at 94.5 cm^{-1} for TiOBr (Fig.2(c)) and at 131.5 cm^{-1} for TiOCl.

The frequency of all the vibrational modes observed for TiOCl and TiOBr in their high temperature phase are summarized in Table I. Here, the infrared active modes are taken from the literature^{7,9} and for the Raman modes the temperatures chosen for the two compounds are 300K for TiOCl and 100K for TiOBr. The observed Raman frequencies agree well with

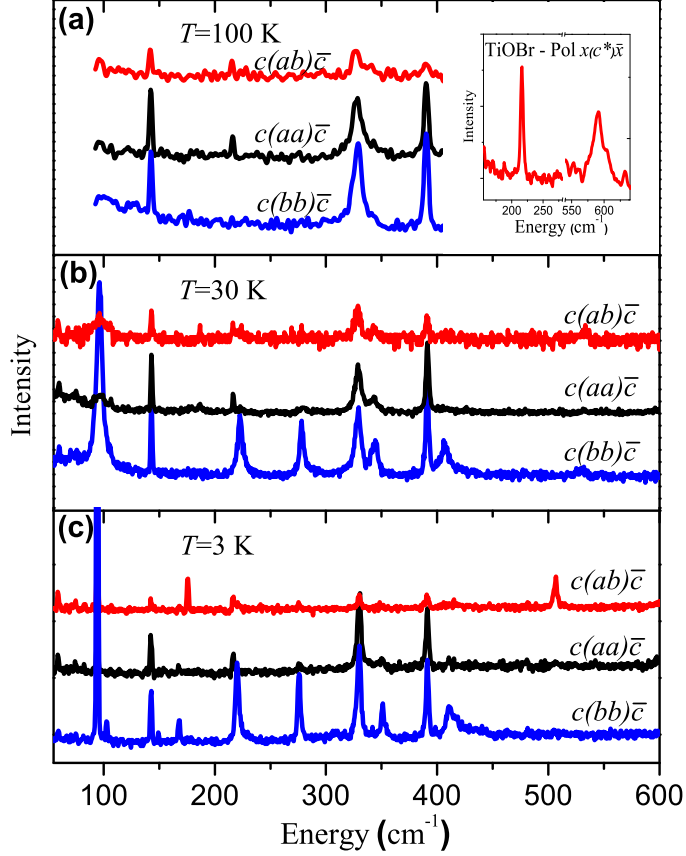


FIG. 2: (Color online) Polarization analysis of the Raman spectra in the three phases of TiOBr, taken at 3 (a), 30 (b) and 100K (c). The spectra of TiOCl show the same main features and closely resemble those of TiOBr. Table IV reports the frequencies of the TiOCl modes. The inset shows the TiOBr spectrum in the $x(c^*)\bar{x}$ polarization (see text).

previous reports¹³. The calculated values reported in Table I are obtained with a spring-model calculation based on phenomenological longitudinal and transversal spring constants (see Appendix). The spring constants used were optimized using the TiOBr experimental frequencies (except for the ones of the B_{3g} modes due to their uncertain symmetry) and kept constant for the other compounds. The frequencies for the other two compounds are obtained by merely changing the appropriate atomic masses and are in good agreement with the experimental values. The relative atomic displacements for each mode of A_g symmetry are shown in Table II. The scaling ratio for the lowest frequency mode (mode 1) between the two compounds is in good agreement with the calculation of the atomic displacements. The low frequency mode is mostly related to Br/Cl movement and, indeed, the ratio $\nu_{TiOCl}/\nu_{TiOBr} = 1.42$ is similar to the mass ratio $\sqrt{M_{Br}}/\sqrt{M_{Cl}}$. The other modes (2 and 3) involve mainly Ti or O displacements, and their frequencies scale with a lower ratio, as can be expected.

B. Low Temperature Phases

Although the symmetry of the low temperature phases has been studied by X-ray crystallography, there is no agreement concerning the symmetry of the SP phase; different works

TABLE I: (a) Vibrational modes for the high temperature phase in TiOCl, TiOBr and VOCl. The calculated values are obtained with a spring model. The mode reported in *italics* in Table I are measured in the $x(c\star)\bar{x}$ polarization they could therefore have either B_{2g} or B_{3g} symmetry (see experimental details).

(a)	TiOBr		TiOCl		VOCl	
	Exp.	Cal.	Exp.	Cal.	Exp.	Cal.
$A_g (\sigma_{aa}, \sigma_{bb}, \sigma_{cc})$	142.7	141	203	209.1	201	208.8
	329.8	328.2	364.8	331.2	384.9	321.5
	389.9	403.8	430.9	405.2	408.9	405.2
$B_{2g}(\sigma_{ac})$		105.5		157.1		156.7
		328.5		330.5		320.5
		478.2		478.2		478.2
$B_{3u}(IR, a)$	77 ^a	75.7	104 ^b	94.4		93.7
	417 ^a	428.5	438 ^b	428.5		425.2
$B_{3g}(\sigma_{bc})$	60	86.4		129.4		129.4
	216	336.8	219 ^c	336.8		327.2
	598	586.3		586.3		585.6
$B_{2u}(IR, b)$	131 ^a	129.1	176 ^b	160.8		159.5
	275 ^a	271.8	294 ^b	272.1		269.8
$B_{1u}(IR, c)$		155.7		194.1		192.4
		304.8		301.1		303.5

^aValue taken from Ref.⁷.

^bValue taken from Ref.⁹.

^cValue obtained considering the leakage in the σ_{yy} polarization.

TABLE II: The ratio between the frequency of the A_g Raman active modes measured in TiOBr and TiOCl is related to the atomic displacements of the different modes as calculated for TiOBr (all the eigenvectors are fully c -polarized, the values are normalized to the largest displacement).

(b)	Mode	$\nu(\text{TiOBr})$	ν_{Cl}/ν_{Br}	Ti	O	Br
	1	142.7	1.42	0.107	0.068	1
	2	329.8	1.11	1	0.003	0.107
	3	389.9	1.11	0.04	1	0.071

proposed two different space groups, $P2_1/m^{14,15,16}$ and $Pmm2^{21}$.

The possible symmetry changes that a dimerisation of Ti ions in the b -direction can cause are considered in order to track down the space group of the TiOX crystals in the low temperature phases. Assuming that the low temperature phases belong to a subgroup of the high temperature orthorhombic space group $Pmmn$, there are different candidate space groups for the low temperature phases. Note that the assumption is certainly correct for the intermediate phase, because the transition at T_{c2} is of second-order implying a symmetry reduction, while it is not necessarily correct for the low temperature phase, being the transition at T_{c1} is of first-order.

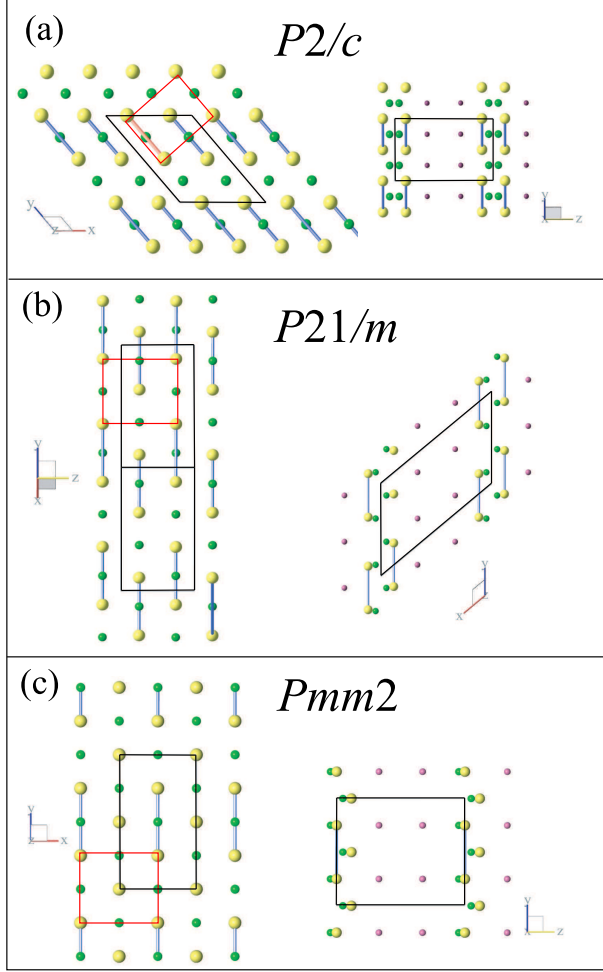


FIG. 3: (Color online) Comparison of the possible low temperature symmetries. The low temperature structures reported are discussed, considering a dimerisation of the unit cell due to Ti-Ti coupling and assuming a reduction of the crystal symmetry. The red rectangle denotes the unit cell of the orthorhombic HT structure. Structure (a) is monoclinic with its unique axis parallel to the orthorhombic c -axis (space group $P2/c$), (b) shows the suggested monoclinic structure for the SP phase ($P2_1/m$), and (c) depicts the alternative orthorhombic symmetry proposed for the low T phase $Pmm2$.

Fig.3 shows a sketch of the three possible low temperature symmetries considered, and Table III reports a summary of the characteristic of the unit cell together with the number of phonons expected to be active for the different space groups. Depending on the relative position of the neighboring dimerised Ti pairs, the symmetry elements lost in the dimerisation are different and the possible space groups in the SP phase are $P2/c$ (Table III(a)), $P2_1/m$ (b) or $Pmm2$ (c). The first two are monoclinic groups with their unique axis perpendicular to the TiO plane (along the c -axis of the orthorhombic phase), and lying in the TiO plane (\parallel to the a -axis of the orthorhombic phase), respectively. The third candidate (Fig.3(c)) has orthorhombic symmetry.

The group theory analysis based on the two space groups suggested for the SP phase ($P2_1/m$ ¹⁴ and $Pmm2$ ²¹) shows that the number of modes expected to be Raman active is

TABLE III: Comparison between the possible low temperature space group.

(a)	Space group $P2/c$ Unique axis \perp to TiO plane, C_{2h}^4 4TiOBr per unit cell $\Gamma = 7A_g + 6A_u + 9B_g + 11B_u$ 7 A_g Raman active $\sigma_{xx}, \sigma_{yy}, \sigma_{zz}, \sigma_{xy}$ 11 B_g Raman active σ_{xz}, σ_{yz} 6 A_u and 9 B_u IR active
(b)	Space group $P2_1/m$ Unique axis in the TiO plane, C_{2h}^2 4 TiOBr per unit cell $\Gamma = 12A_g + 5A_u + 6B_g + 10B_u$ 12 A_g Raman active $\sigma_{xx}, \sigma_{yy}, \sigma_{zz}, \sigma_{xy}$ 6 B_g Raman active σ_{xz}, σ_{yz} 5 A_u and 10 B_u IR active
(c)	Space group $Pmm2$ 4 TiOBr per unit cell $\Gamma = 11A_1 + A_2 + 4B_1 + 5B_2$ 11 A_1 Raman active $\sigma_{xx}, \sigma_{yy}, \sigma_{zz}$ A_2 Raman active σ_{xy} 4 B_1 and 5 B_2 Raman active in σ_{xz} and σ_{yz}

different in the two cases (Table III(b) and (c)). In particular, the 12 fully symmetric vibrational modes (A_g), in the $P2_1/m$ space group, are expected to be active in the $\sigma_{xx}, \sigma_{yy}, \sigma_{zz}$ and σ_{xy} polarizations, and 6 B_g modes are expected to be active in the cross polarizations (σ_{xz} and σ_{yz}). Note that in this notation, z refers to the unique axis of the monoclinic cell, so σ_{yz} corresponds to $c(ab)c$ for the HT orthorhombic phase. For $Pmm2$ the 11 A_1 vibrational modes are expected to be active in the $\sigma_{xx}, \sigma_{yy}, \sigma_{zz}$ polarizations, and only one mode of symmetry A_2 is expected to be active in the cross polarization (σ_{xy} or $c(ab)c$). The experiments, reported in Table IV for both compounds and in Fig.2 for TiOBr only, show that 10 modes are active in the $c(aa)c$ and $c(bb)c$ in the SP phase (Fig.2(c)), and, more importantly, two modes are active in the cross polarization $c(ab)c$. This is not compatible with the expectation for $Pmm2$. Hence the comparison between the experiments and the group theoretical analysis clearly shows that of the two low temperature structures reported in X-ray crystallography^{15,21}, only the $P2_1/m$ is compatible with the present results.

As discussed in the introduction, the presence of three phases in different temperature intervals for TiOX is now well established even though the nature of the intermediate phase is still largely debated^{7,12,15}. The temperature dependence of the Raman active modes for TiOBr between 3 and 50 K, is depicted in Fig.4. In the spin-Peierls phase, as discussed above, the reduction of the crystal symmetry¹⁶ increases the number of Raman active modes. Increasing the temperature above T_{c1} a different behavior for the various low temperature phonons is observed. As shown in Fig.4, some of the modes disappear suddenly at T_{c1} (labeled L_T), some stay invariant up to the HT phase (R_T) and some others undergo a sudden broadening at T_{c1} and slowly disappear upon approaching T_{c2} (I_T). The polarization analysis of the Raman modes in the temperature region $T_{c1} < T < T_{c2}$ shows that the number

TABLE IV: Vibrational modes of the low temperature phases.

spin Peierls phase							
(a)	TiOBr	$A_g(\sigma_{xx}, \sigma_{yy})$	94.5	102.7	142.4	167	219
			276.5	330	351	392	411*
	TiOCl	$A_g(\sigma_{xy})$	175.6	506.5			
		$A_g(\sigma_{xx}, \sigma_{yy})$	131.5	145.8	203.5	211.5	296.5
		$A_g(\sigma_{xy})$	305.3	322.6	365.1	387.5	431*
			178.5	524.3			
Intermediate phase							
(b)	TiOBr (30K)	$A_g(\sigma_{xx}, \sigma_{yy})$	94.5	142	221.5	277	328.5
			344.5	390.4			
	TiOCl (75K)	$A_g(\sigma_{xx}, \sigma_{yy})$	132.8	206.2	302	317.2	364.8
			380	420.6			

* The broad line shape of this feature suggests it may originate from a two-phonon process.

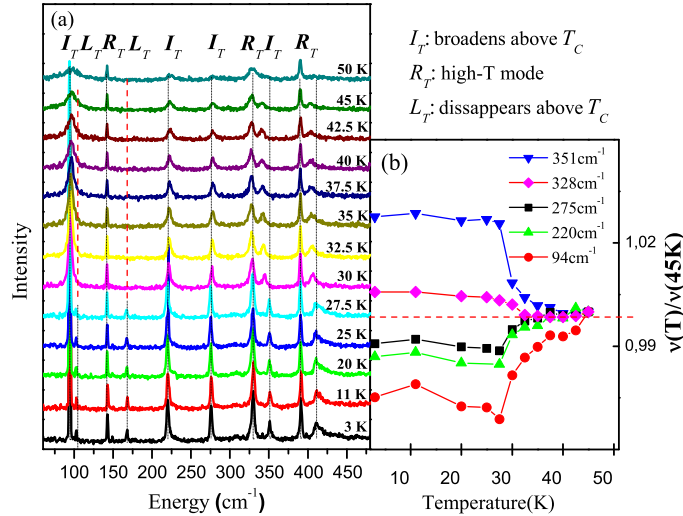


FIG. 4: (Color online) The temperature dependence of the Raman spectrum of TiOBr is depicted (an offset is added for clarity). The 3 modes present at all temperatures are denoted by the label R_T . The modes characteristic of the low temperature phase (disappearing at $T_{c1} = 28$ K) are labelled L_T , and the anomalous modes observed in both the low temperature and the intermediate phase are labelled I_T . The right panel (b) shows the behavior of the frequency of I_T modes, plotted renormalized to their frequency at 45 K. It is clear that the low-frequency modes shift to higher energy while the high-frequency modes shift to lower frequency.

of active modes in the intermediate phase is different from that in both the HT and the SP phases. The fact that at $T = T_{c1}$ some of the modes disappear suddenly while some others do not disappear, strongly suggests that the crystal symmetry in the intermediate phase is different from both other phases, and indeed confirms the first-order nature of the transition at T_{c1} .

In the X-ray structure determination¹⁵, the intermediate incommensurate phase is discussed in two ways. Firstly, starting from the HT orthorhombic ($Pmmn$) and the SP monoclinic space group ($P2_1/m$ - unique axis in the TiO planes, \parallel to a), the modulation vector required to explain the observed incommensurate peaks is two-dimensional for both space groups. Secondly, starting from another monoclinic space group, with unique axis perpendicular to the TiO bilayers ($P2/c$), the modulation vector required is one-dimensional. The latter average symmetry is considered (in the commensurate variety) in Fig.3(a) and Table III(a).

In the IP, seven modes are observed in the σ_{xx} , σ_{yy} and σ_{zz} geometry on both compounds (see Table IV(b)), and none in the σ_{xy} geometry. This appears to be compatible with all the space groups considered, and also with the monoclinic group with unique axis perpendicular to the TiO planes (Table III(a)). Even though from the evidence it is not possible to rule out any of the other symmetries discussed, the conjecture that in the intermediate incommensurate phase the average crystal symmetry is already reduced, supports the description of the intermediate phase as a monoclinic group with a one-dimensional modulation¹⁵, and moreover it explains the anomalous first-order character of the spin-Peierls transition at T_{c1} . The diagram shown in Fig.5 aims to visualize that the space group in the spin-Peierls state

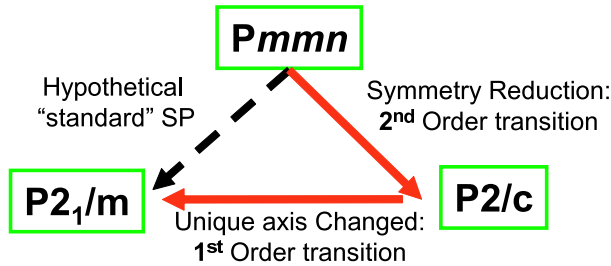


FIG. 5: (Color online) The average crystal symmetry of the intermediate phase is proposed to be monoclinic with the unique axis parallel to the c -axis of the orthorhombic phase. Hence the low temperature space group is not a subgroup of the intermediate phase, and the transition to the spin-Peierls phase is consequently of first order.

($P2_1/m$) is a subgroup of the high temperature $Pmmn$ group, but not a subgroup of any of the possible intermediate phase space groups suggested (possible $P2/c$). This requires the phase transition at T_{c1} to be of first order, instead of having the conventional spin-Peierls second-order character.

Let us return to Fig.4(b) to discuss another intriguing vibrational feature of the intermediate phase. Among the modes characterizing the intermediate phase (I_T), the ones at low frequency shift to higher energy approaching T_{c2} , while the ones at high frequency move to lower energy, seemingly converging to a central frequency ($\simeq 300 \text{ cm}^{-1}$ for both TiOCl and TiOBr). This seems to indicate an interaction of the phonons with some excitation around 300 cm^{-1} . Most likely this is in fact arising from a strong, thermally activated coupling of the lattice with the magnetic excitations, and is consistent with the pseudo-spin gap observed in NMR experiments^{4,22} of $\approx 430 \text{ K}$ ($\simeq 300 \text{ cm}^{-1}$).

C. Magnetic Interactions

As discussed in the introduction, due to the shape of the singly occupied $3d$ orbital, the main magnetic exchange interaction between the spins on the Ti ions is along the crystallographic b -direction. This, however, is not the only effective magnetic interaction. In fact,

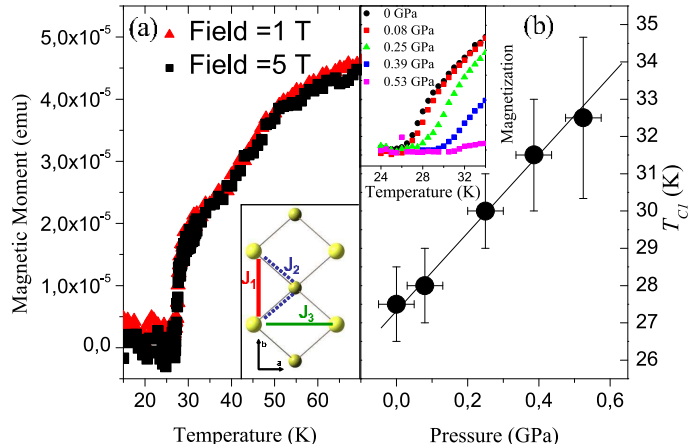


FIG. 6: (Color online) (a) Magnetization as a function of temperature measured with fields 1 T and 5 T (the magnetization measured at 1 T is multiplied by a factor of 5 to evidence the linearity). The inset shows the main magnetic interactions (see text). (b) Pressure dependence of T_{c1} . The transition temperature for transition to the spin-Peierls phase increases with increasing pressure. The inset shows the magnetization versus the temperature after subtracting the background signal coming from the pressure cell.

one also expects a superexchange interaction between nearest and next-nearest neighbor chains (J_2 and J_3 in the insert of Fig.6(a))²³. The situation of TiOX is made more interesting by the frustrated geometry of the interchain interaction, where the magnetic coupling J_2 between adjacent chains is frustrated and the exchange energies can not be simultaneously minimized. Table V reports the exchange interaction values for the three possible magnetic interactions calculated for TiOBr. These magnetic interactions were computed with a DFT Broken symmetry approach²⁴ using an atom cluster including the two interacting atoms and all the surrounding ligand atoms, in addition the first shell of Ti^{3+} ions was replaced by Al^{3+} ions and also included in the cluster. The calculations were performed with the Gaussian03 package²⁵ using the hybrid exchange-correlation functional B3LYP²⁶ and the 6-3111G* basisset.

TABLE V: Calculated Exchange interactions in TiOBr

TiOBr
$J_1 = -250$ K
$J_2 = -46.99$ K
$J_3 = 11.96$ K

Although the computed value for the magnetic interaction along the b -axis is half of the value obtained from the magnetic susceptibility fitted with a Bonner-Fisher curve accounting

for a one-dimensional Heisenberg chain, it is possible to extract some conclusions from the ab-initio computations. The most interesting outcome of the results is that in addition to the magnetic interaction along the b -axis, there is a relevant interchain interaction ($J_1/J_2 = 5.3$) in TiOBr. Firstly, this explains the substantial deviation of the Bonner-Fisher fit from the magnetic susceptibility even at temperature higher than T_{c2} . Secondly, the presence of an interchain interaction, together with the inherent frustrated geometry of the bilayer structure, was already proposed in literature¹² in order to explain the intermediate phase and its structural incommensurability.

The two competing exchange interactions J_1 and J_2 have different origins: the first arises from direct exchange between Ti ions, while the second is mostly due to the superexchange interaction through the oxygen ions²³. Thus, the two exchange constants are expected to depend differently on the structural changes induced by hydrostatic pressure, J_1 should increase with hydrostatic pressure (increases strongly with decreasing the distance between the Ti ions), while J_2 is presumably weakly affected due only to small changes in the Ti-O-Ti angle (the compressibility estimated from the lattice dynamics simulation is similar along the a and b crystallographic directions). The stability of the fully dimerized state is reduced by the presence of an interchain coupling, so that T_{c1} is expected to be correlated to J_1/J_2 . Pressure dependent magnetic experiments have been performed to monitor the change of T_{c1} upon increasing hydrostatic pressure. The main results, shown in Fig.6, indeed is consistent with this expectation: T_{c1} increases linearly with pressure; unfortunately it is not possible to address the behavior of T_{c2} from the present measurements.

D. Electronic Excitations and Comparison with VOCl

The nature of the complex phase diagram of TiOX was originally tentatively ascribed to the interplay of spin, lattice and orbital degrees of freedom⁷. Only recently, infrared spectroscopy supported by cluster calculations excluded a ground state degeneracy of the Ti d orbitals for TiOCl, hence suggesting that orbital fluctuations can not play an important role in the formation of the anomalous incommensurate phase^{27,28}. Since the agreement between the previous cluster calculations and the experimental results is not quantitative, the energy of the lowest $3d$ excited level is not accurately known, not allowing to discard the possibility of an almost degenerate ground state. For this reason a more formal cluster calculation has been performed using an embedded cluster approach. In this approach a TiO₂Cl₄ cluster was treated explicitly with a CASSCF/CASPT2 quantum chemistry calculation. This cluster was surrounded by eight Ti³⁺ TIP potentials in order to account for the electrostatic interaction of the cluster atoms with the shell of the first neighboring atoms. Finally, the cluster is embedded in a distribution of punctual charges fitting the Madelung's potential produced by the rest of the crystal inside the cluster region. The calculations were performed using the MOLCAS quantum chemistry package²⁹ with a triple quality basis set; for the Ti atom polarization functions were also included. The calculations reported in Table VI, confirmed the previously reported result²⁷ for both TiOCl and TiOBr. The first excited state d_{xy} is at 0.29-0.3 eV (> 3000 K) for both compounds, therefore the orbital degrees of freedom are completely quenched at temperatures close to the phase transition.

A comparison with the isostructural compound VOCl has been carried out to confirm that the phase transitions of the TiOX compounds are intimately related to the unpaired $S=1/2$ spin of the Ti ions. The V³⁺ ions have a $3d^2$ electronic configuration. Each ion carries two unpaired electrons in the external d shell, and has a total spin of 1. The crystal

TABLE VI: Crystal field splitting of $3d^1$ Ti^{3+} in TiOCl and TiOBr (eV).

	TiOCl	TiOBr
xy	0.29-0.29	0.29-0.30
xz	0.66-0.68	0.65-0.67
yz	1.59-1.68	1.48-1.43
$x^2 - y^2$	2.30-2.37	2.21-2.29

field environment of V^{3+} ions in VOCl is similar to that of Ti^{3+} in TiOX , suggesting that the splitting of the degenerate d orbital could be comparable. The electrons occupy the two lowest t_{2g} orbitals, of $d_{y^2-z^2}$ (responsible for the main exchange interaction in TiOX) and d_{xy} symmetry respectively. Where the lobes of the latter point roughly towards the Ti^{3+} ions of the nearest chain (Table VI). It is therefore reasonable to expect that the occupation of the d_{xy} orbital in VOCl leads to a substantial direct exchange interaction between ions in different chains in VOCl and thus favors a two-dimensional antiferromagnetic order. Indeed, the magnetic susceptibility is isotropic at high temperatures and well described by a quadratic two-dimensional Heisenberg model, and at $T_N = 80$ K VOCl undergoes a phase transition to a two-dimensional antiferromagnet³⁰.

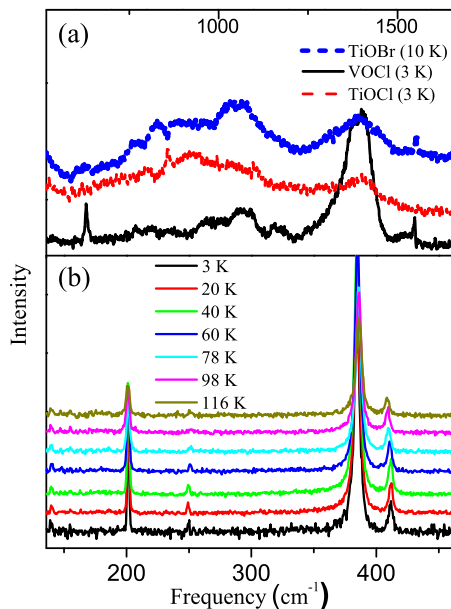


FIG. 7: (Color online) Raman scattering features of VOCl . (a) High energy scattering of TiOCl/Br and VOCl , and (b) temperature dependence of the vibrational scattering features of VOCl . No symmetry changes are observed at $T_N = 80$ K.

The space group of VOCl at room temperature is the same as that of TiOX in the high temperature phase ($Pm\bar{m}n$), and, as discussed in the previous section, three A_g modes are expected to be Raman active. As shown in Fig.7(b), three phonons are observed throughout the full temperature range (3 – 300 K), and no changes are observed at T_N . The modes observed are consistent with the prediction of lattice dynamics calculations (Table I).

In the energy region from 600 to 1500 cm^{-1} , both TiOBr and TiOCl show a similar

highly structured broad scattering continuum, as already reported in literature^{13,19}. The fact that the energy range of the anomalous feature is consistent with the magnetic exchange constant in TiOCl ($J=660$ K) suggested at first an interpretation in terms of two-magnon Raman scattering¹³. Later it was shown that the exchange constant estimated for TiOBr is considerably smaller ($J=406$ K) with respect to that of TiOCl while the high energy scattering stays roughly at the same frequency. Even though the authors of ref.¹⁹ still assigned the scattering continuum to magnon processes, it seems clear that the considerably smaller exchange interaction in the Br compound ($J=406$ K) falsifies this interpretation and that magnon scattering is not at the origin of the high energy scattering of the two compounds. Furthermore, the cluster calculation (Table VI) clearly shows that no excited crystal field state is present in the energy interval considered, ruling out a possible orbital origin for the continuum. These observations are further strengthened by the observation of a similar continuum scattering in VOCl (see fig. 7(a)) which has a different magnetic and electronic nature. Therefore, the high energy scattering has most likely a vibrational origin. The lattice dynamics calculations, confirmed by the experiments, show that a "high" energy mode ($\simeq 600$ cm⁻¹) of symmetry B_{3g} (Table I) is expected to be Raman active in the σ_{yz} polarization. Looking back at Fig.2, the inset shows the measurements performed with the optical axis parallel to the TiOX plane, where the expected mode is observed at 598 cm⁻¹. The two phonon process related to this last intense mode is in the energy range of the anomalous scattering feature and has symmetry A_g ($B_{3g} \otimes B_{3g}$). The nature of the anomalies observed is therefore tentatively ascribed to a multiple-phonon process. Further detailed investigations of lattice dynamics are needed to clarify this issue.

IV. CONCLUSION

The symmetry of the different phases has been discussed on the basis of inelastic light scattering experiments. The high temperature Raman experiments are in good agreement with the prediction of the group theoretical analysis (apart from one broad mode which is ascribed to pre-transitional fluctuations). Comparing group theoretical analysis with the polarized Raman spectra clarifies the symmetry of the spin-Peierls phase and shows that the average symmetry of the incommensurate phase is different from both the high temperature and the SP phases. The conjecture that the intermediate phase is compatible with a different monoclinic symmetry (unique axis perpendicular to the TiO planes) could explain the anomalous first-order character of the transition to the spin-Peierls phase. Moreover, an anomalous behavior of the phonons characterizing the intermediate phase is interpreted as evidencing an important spin-lattice coupling. The susceptibility measurements of TiOBr show that T_{c1} increases with pressure, which is ascribed to the different pressure dependence of intrachain and interchain interactions. Finally, we compared the TiOX compounds with the "isostructural" VOCl. The presence of the same anomalous high energy scattering feature in all the compounds suggests that this feature has a vibrational origin rather than a magnetic or electronic one.

Acknowledgements The authors are grateful to Maxim Mostovoy, Michiel van der Vegte, Paul de Boeij, Daniel Khomskii, Iberio Moreira and Markus Grüninger for valuable and insightful discussions. This work was partially supported by the Stichting voor Fundamenteel Onderzoek der Materie [FOM, financially supported by the Nederlandse Organisatie voor Wetenschappelijk Onderzoek (NWO)], and by the German Science Foundation (DFG).

V. APPENDIX: DETAILS OF THE SPRING MODEL CALCULATION

The spring model calculation reported in the paper, was carried out using the software for lattice-dynamical calculation UNISOFT³¹ (release 3.05). In the calculations the Born-von Karman model was used; here the force constants are treated as model parameters and they are not interpreted in terms of a special interatomic potential. Only short range interactions between nearest neighbor ions are taken into account. Considering the forces to be central forces, the number of parameters is reduced to two for each atomic interaction: the longitudinal and transversal forces respectively defined as $L = \frac{d^2V(\bar{r}_{i,j})}{dr^2}$ and $T = \frac{1}{r} \frac{dV(\bar{r}_{i,j})}{dr}$. A custom made program was interfaced with UNISOFT to optimize the elastic constants. Our program proceeded scanning the n dimensional space ($n =$ number of parameters) with a discrete grid, to minimize the squared difference between the calculated phonon frequencies and the measured experimental frequencies for TiOBr, taken from both Raman and infrared spectroscopy. The phonon frequencies of TiOCl and VOCl were obtained using the elastic constants optimized for TiOBr and substituting the appropriate ionic masses. The optimized force constants between different atoms are reported in N/m in the following Table.

TABLE VII: Elastic constants used in the spring model calculation. The label numbers refer to Fig. ??, while the letters refer to the different inequivalent positions of the ions in the crystal.

Number	Ions	Longitudinal (L) (N/m)	Transversal (T) (N/m)
1	Ti(a)-Ti(b)	18.5	32.7
2	Ti(a)-O(a)	18.5	11.1
3	Ti(a)-O(b)	53.1	9.5
4	Ti(a)-X(a)	29.0	4.4
5	O(a)-O(b)	20.6	7.3
6	X(a)-O(a)	18.5	3.5
7	X(a)-X(b)	11.7	0.7

* Electronic address: d.fausti@rug.nl

† Electronic address: P.H.M.van.Loosdrecht@rug.nl

¹ M. Imada, A. Fujimori, and Y. Tokura, Rev. Mod. Phys. **70**, 1039 (1998).

² E. Dagotto, Rep. Prog. Phys. **62**, 1525 (1999).

³ V. Kataev, J. Baier, A. Möller, L. Jongen, G. Meyer, , and A. Freimuth, Phys. Rev. B **68**, 140405 (2003).

⁴ T. Imai and F. C. Choub, cond-mat **0301425** (2003), URL <http://xxx.lanl.gov/abs/cond-mat/0301425>.

⁵ C. H. Maule, J. N. Tothill, P. Strange, and J. A. Wilson, J. Phys. C **21**, 2153 (1988).

⁶ A. Seidel, C. A. Marianetti, F. C. Chou, G. Ceder, and P. A. Lee, Phys. Rev. B **67**, 020405 (2003).

⁷ G. Caimi, L. Degiorgi, P. Lemmens, and F. C. Chou, J. Phys. Cond. Mat. **16**, 5583 (2004).

⁸ R. J. Beynon and J. A. Wilson, J. Phys. Cond. Mat. **5**, 1983 (1993).

- ⁹ G. Caimi, L. Degiorgi, N. N. Kovaleva, P. Lemmens, and F. C. Chou, Phys. Rev. B **69**, 125108 (2004).
- ¹⁰ M. Shaz, S. van Smaalen, L. Palatinus, M. Hoinkis, M. Klemm, S. Horn, and R. Claessen, Phys. Rev. B **71**, 100405 (2005).
- ¹¹ J. Hemberger, M. Hoinkis, M. Klemm, M. Sing, R. Claessen, S. Horn, and A. Loidl, Phys. Rev. B **72**, 012420 (2005).
- ¹² R. Rückamp, J. Baier, M. Kriener, M. W. Haverkort, T. Lorenz, G. S. Uhrig, L. Jongen, A. Möller, G. Meyer, and M. Grüninger, Phys. Rev. Lett. **95**, 097203 (2005).
- ¹³ P. Lemmens, K. Y. Choi, G. Caimi, L. Degiorgi, N. N. Kovaleva, A. Seidel, and F. C. Chou, Phys. Rev. B **70**, 134429 (2004).
- ¹⁴ L. Palatinus, A. Schoenleber, and S. van Smaalen, Acta Crystallogr. Sect. C **61**, 148 (2005).
- ¹⁵ S. van Smaalen, L. Palatinus, and A. Schoenleber, Phys. Rev. B **72**, 020105(R) (2005).
- ¹⁶ A. Schoenleber, S. van Smaalen, and L. Palatinus, Phys. Rev. B **73**, 214410 (2006).
- ¹⁷ A. Krimmel, J. Stempffer, B. Bohnenbuck, B. Keimer, M. Hoinkis, M. Klemm, S. Horn, A. Loidl, M. Sing, R. Claessen, et al., Phys. Rev. B **73**, 172413 (2006).
- ¹⁸ C. A. Kuntscher, S. Frank, A. Pashkin, M. Hoinkis, M. Klemm, M. Sing, S. Horn, and R. Claessen, Phys. Rev. B **74**, 184402 (2006).
- ¹⁹ P. Lemmens, K. Y. Choi, R. Valenti, T. Saha-Dasgupta, E. Abel, Y. S. Lee, and F. C. Chou, New Journal of Physics **7**, 74 (2005).
- ²⁰ D. L. Rousseau, R. P. Bauman, and S. P. S. Porto, Journal of Raman Spectroscopy **10**, 253 (1981).
- ²¹ T. Sasaki, T. Nagai, K. Kato, M. Mizumaki, T. Asaka, M. Takata, Y. Matsui, H. Sawa, and J. Akimitsu, Sci. Tech. Adv. Mat. **7**, 17 (2006).
- ²² P. J. Baker, S. J. Blundell, F. L. Pratt, T. Lancaster, M. L. Brooks, W. Hayes, M. Isobe, Y. Ueda, M. Hoinkis, M. Sing, et al., Phys. Rev. B **75**, 094404 (2007).
- ²³ R. Macovez (2007), unpublished.
- ²⁴ L. Noodleman and J. G. Norman, J. Chem. Phys. **70**, 4903 (1979).
- ²⁵ M. J. F. et al., *Gaussian 03, revision c.02*, gaussian, Inc., Wallingford, CT, 2004.
- ²⁶ A. D. Becke, J. Chem. Phys. **98**, 5648 (1993).
- ²⁷ R. Rückamp, E. Benckiser, M. W. Haverkort, H. Roth, T. Lorenz, A. Freimuth, L. Jongen, A. Möller, G. Meyer, P. Reutler, et al., New Journal of Physics **7**, 1367 (2005).
- ²⁸ D. V. Zakharov, J. Deisenhofer, H. A. K. von Nidda, P. Lunkenheimer, J. Hemberger, M. Hoinkis, M. Klemm, M. Sing, R. Claessen, M. V. Eremin, et al., Phys. Rev. B **73**, 094452 (2006).
- ²⁹ G. Karlstro, R. Lindh, P. Malmqvist, B. Roos, U. Ryde, V. Veryazov, P. Widmark, M. Cossi, B. Schimmelpfennig, P. Neogrady, et al., Comput. Mater. Sci. **28**, 222 (2003).
- ³⁰ A. Wiedenmann, J. R. Mignod, J. P. Venien, and P. Palvadeau, JMMM **45**, 275 (1984).
- ³¹ G. Eckold, *UNISOFT - A Program Package for Lattice Dynamical Calculations: Users Manual* (1992).